JAIST Repository
https://dspace.jaist.ac.jp/

Title	Towards designing Mn_4 molecules with strong intramolecular exchange coupling
Author(s)	Nguyen, Anh Tuan; Dam, Hieu Chi
Citation	Advances in Natural Sciences: Nanoscience and Nanotechnology, 2(1): 015011
Issue Date	2011-03-08
Type	Journal Article
Text version	publisher
URL	http://hdl.handle.net/10119/10312
Rights	Copyright (C) 2011 Vietnam Academy of Science & Technology. Anh Tuan Nguyen and Hieu Chi Dam, Advances in Natural Sciences: Nanoscience and Nanotechnology, 2(1), 2011, 015011. http://dx.doi.org/10.1088/2043-6262/2/1/015011
Description	

JAIST
JAPAN
ADVANCED INSTITUTE OF
SCIENCE AND TECHNOLOGY

Japan Advanced Institute of Science and Technology

Adv. Nat. Sci.: Nanosci. Nanotechnol. **2** (2011) 015011 (8pp) doi:10.1088/2043-6262/2/1/015011

Towards designing Mn_4 molecules with strong intramolecular exchange coupling

Anh Tuan Nguyen[1] **and Hieu Chi Dam**[1,2]

[1] Faculty of Physics, Hanoi University of Science, Vietnam National University, 334 Nguyen Trai, Thanh Xuan District, Hanoi, Vietnam
[2] School of Materials Science, Japan Advanced Institute of Science and Technoloy, 1-1, Asahidai, Nomi, Ishikawa, 923-1292 Japan

E-mail: tuanna@hus.edu.vn

Received 10 October 2010
Accepted for publication 14 February 2011
Published 8 March 2011
Online at stacks.iop.org/ANSN/2/015011

Abstract
Distorted cubane $Mn^{4+}Mn^{3+}_3$ single-molecule magnets (SMMs) have been studied by first-principles calculations, i.e. $[Mn_4L_3X(OAc)_3(dbm)_3]$ (L = O; X = F, Cl, and Br; dbmH = dibenzoyl-methane). It was shown in our previous paper (Tuan *et al* 2009 *Phys. Chem. Chem. Phys.* **11** 717) that the ferrimagnetic structure of $Mn^{4+}Mn^{3+}_3$ SMMs is dominated by π type hybridization between the d_{z^2} orbitals at the three high-spin Mn^{3+} ions and the t_{2g} orbitals at the Mn^{4+} ion. To design new $Mn^{4+}Mn^{3+}_3$ molecules having much more stable ferrimagnetic states, one approach is suggested. This involves controlling the Mn^{4+}–L–Mn^{3+} exchange pathways by rational variations in ligands to strengthen the hybridization between the Mn ions. Based on this method, we succeed in designing new distorted cubane $Mn^{4+}Mn^{3+}_3$ molecules having Mn^{4+}–Mn^{3+} exchange coupling of about 3 times stronger than that of the synthesized $Mn^{4+}Mn^{3+}_3$ molecules. These results give some hints regarding experimental efforts to synthesize new superior $Mn^{4+}Mn^{3+}_3$ SMMs.

Keywords: single-molecule magnets, first-principles calculation, computational materials design

Classification numbers: 2.01, 3.02, 4.00, 5.02

1. Introduction

High-spin molecules that can function as magnets below their blocking temperature (T_B) are being studied extensively due to their potential technological applications to molecular spintronics [1]. These molecules display slow magnetic relaxation below their T_B, and such molecules have been called single-molecule magnets (SMMs) [2]. This behavior results from a high ground-state spin (S_T) combined with a large and negative Ising type of magnetoanisotropy, as measured by the axial zero-field splitting parameter (D). This combination leads to a significant barrier (U) to magnetization reversal, whose maximum value is given by $U = -DS_T^2$ for integer spin and $U = -D(S_T^2 - 1/4)$ for half integer spin.

SMMs consist of magnetic atoms connected and surrounded by ligands. The challenge of SMMs consists in tailoring their magnetic properties by specific modifications of the molecular units. As described above, S_T and D are the important parameters for the control of SMM behavior. The D depends on designing the local anisotropies of the single ions, such as Mn^{3+} ion, and their vectorial addition to give a resulting anisotropy. The S_T results from local spin moments at TM ions (S_i) and exchange coupling between them (J_{ij}) effectively. Moreover, J_{ij} has to be important to separate the ground spin state from the excited states; the relative high values of U and T_B are dependent on them [3]. However, currently synthesized SMMs usually have weak J_{ij}, of the order of several tens of Kenvil or much smaller [4]. Therefore, seeking possibilities for the enhancement of J_{ij} will be very valuable in the development of SMMs.

In the framework of computational materials design, distorted cubane $Mn^{4+}Mn^{3+}_3$ SMMs are one of the most attractive SMM systems because their interesting geometric structure and important magnetic quantities can be estimated accurately from first-principles calculations [5, 6].

In experiment, much effort has been spent on synthesizing new distorted cubane $[Mn^{4+}Mn^{3+}_3(\mu_3\text{-}O^{2-})_3(\mu_3\text{-}X^-)(O_2CR)^-_3(L1, L2)^-_3]$ SMMs by varying

 © 2011 Vietnam Academy of Science & Technology

the core X group (X^- = an anionic ligand), the R group (R = a radical such as CH_3 or C_2H_5), or the peripheral-ligands group (L1,L2) = (py,Cl) or (dbm). However, with these variations, the exchange coupling parameters between Mn ions are still of the order of several ten Kenvil [7–15].

Among various distorted cubane $Mn^{4+}Mn^{3+}_3$ SMMs, the previous theoretical studies focused on $Mn^{4+}Mn^{3+}_3(\mu_3\text{-}O^{2-})_3(\mu_3\text{-}Cl^-)(O_2CMe)^-_3(dbm)^-_3$ (hereafter Mn_4-dbm, with dbmH =dibenzoyl-methane) and the dimer $[Mn^{4+}Mn^{3+}_3(\mu_3\text{-}O^{2-})_3(\mu_3\text{-}Cl^-)(O_2CEt)^-_3(py, Cl)^-_3]_2$ [5, 6]. Their electronic structures have been investigated. Also, their important magnetic parameters, such as the ground state spin and effective exchange-coupling parameters, have been calculated. In general, the previous calculated results were in good agreement with experiment. In particular, in our previous paper [5], by using first-principles calculations within generalized gradient approximation (GGA), we analyzed the basic mechanism in the antiferromagnetic (AFM) interaction between the Mn^{4+} ion and the three high-spin Mn^{3+} ions in $Mn^{4+}Mn^{3+}_3$ SMMs. The AFM Mn^{4+}–Mn^{3+} coupling (J_{AB}) is determined by the π type hybridization states among the d_{z^2} orbitals at the Mn^{3+} sites and the t_{2g} orbitals at the Mn^{4+} site through the p orbitals at the μ_3-O^{2-} ions. Therefore, the strength of this coupling is expected to be sensitive to the change in Mn^{4+}–μ_3-O^{2-}–Mn^{3+} angle (α), and strongest with $\alpha \approx 90^\circ$. This finding shows that the Mn^{4+}–Mn^{3+} coupling of distorted cubane $Mn^{4+}Mn^{3+}_3$ SMMs can be structurally controlled. Moreover, until now, synthesized $Mn^{4+}Mn^{3+}_3$ molecules have $\alpha \approx 95^\circ$ [7–15]. Therefore, seeking $Mn^{4+}Mn^{3+}_3$ molecules with $\alpha \approx 90^\circ$ is an effective way to develop new, superior $Mn^{4+}Mn^{3+}_3$ SMMs with strong intramolecular exchange coupling. This can be made by rational variations of ligands.

Here we present our exploration of the control of J_{AB} of distorted cubane $Mn^{4+}Mn^{3+}_3$ SMMs. By rational variations of the μ_3-O, μ_3-Cl, O_2CMe, and dbm groups of the synthesized Mn_4-dbm or $Mn^{4+}Mn^{3+}_3(\mu_3\text{-}O^{2-})_3(\mu_3\text{-}Cl^-)(O_2CMe)^-_3(dbm)^-_3$ molecule, 42 distorted cubane $Mn^{4+}Mn^{3+}_3$ molecules have been designed. Their geometric structure, electronic structure and J_{AB} were investigated by using DMol^3 code based on density functional theory (DFT) [16]. Our calculated results show that significant changes in the exchange pathways between the Mn^{4+} and Mn^{3+} ions as well as J_{AB} can be made by substitutions of N-based ligands (NR′, R′ = a radical) for the bridging ligand μ_3-O^{2-}. By combining these ligand variations, J_{AB} can be enhanced by a factor of 3. This finding is very valuable, since it gives us a method to control exchange couplings of not only the specific system studied in this paper but also other transition metal complexes. Therefore, our results should facilitate the rational synthesis of new SMMs and, eventually, the preparation of technologically useful SMMs.

2. Computational method

All calculations have been performed by using DMol^3 code with the double numerical basis sets plus polarization functional (DNP) [16]. For the exchange correlation terms, the generalized gradient approximation (GGA) RPBE functional was used [17]. An all-electron relativistic Hamiltonian was used to describe the interaction between the core and valence electrons [18]. The real-space global cutoff radius was set to 4.7 Å for all atoms. The spin-unrestricted DFT was used to obtain all results presented in this study. The atomic charge and magnetic moment were obtained by using the Mulliken population analysis [19]. For better accuracy, the octupole expansion scheme was adopted to resolve the charge density and Coulombic potential, and a fine grid was chosen for numerical integration. The charge density was converged to 1×10^{-6} a.u. in the self-consistent calculation. In the optimization process, the energy, energy gradient and atomic displacement were converged to 1×10^{-5}, 1×10^{-4} and 1×10^{-3} a.u., respectively. In order to determine the ground-state atomic structure of each Mn_4 SMM, we carried out total-energy calculations with full geometry optimization, allowing the relaxation of all atoms in molecules.

The exchange coupling parameters of Mn_4 molecules were calculated using the total energy difference method [5].

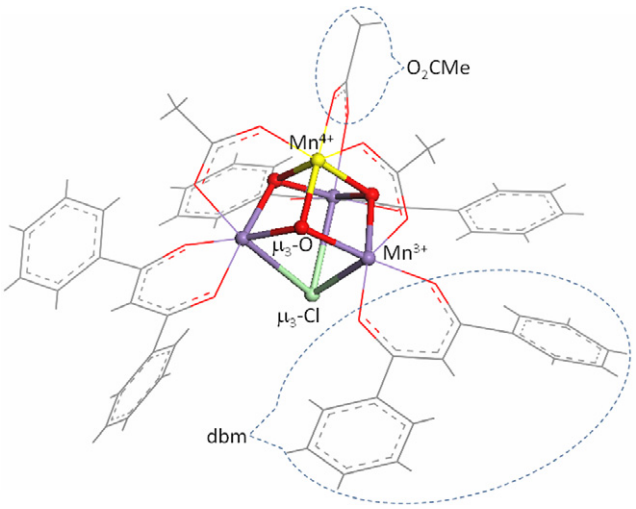

Figure 1. The schematic geometric structure of $[Mn^{4+}Mn^{3+}_3(\mu_3\text{-}O^{2-})_3(\mu_3\text{-}Cl^-)(O_2CMe)^-_3(dbm)^-_3]$ molecules (the atoms in the distorted cubane $[Mn^{4+}Mn^{3+}_3(\mu_3\text{-}O^{2-})_3(\mu_3\text{-}Cl^-)]$ core are highlighted in the ball).

3. Results and discussion

The geometric structure of a synthesized $[Mn^{4+}Mn^{3+}_3(\mu_3\text{-}O^{2-})_3(\mu_3\text{-}Cl^-)(O_2CMe)^-_3(dbm)^-_3]$ molecule is depicted in figure 1. Previous experimental studies reported that each molecule has C_{3v} symmetry, with the C_3 axis passing through Mn^{4+} and X^- ions [12]. The $[Mn^{4+}Mn^{3+}_3(\mu_3\text{-}O)_3(\mu_3\text{-}X)]$ core can be viewed simply as a 'distorted cubane', in which the four Mn atoms are located at the corners of a trigonal pyramid, with a μ_3-O^{2-} ion bridging each of the vertical faces and a μ_3-Cl^- ion bridging the basal face. Three carboxylate (O_2CMe) groups, forming three bridges between the A site (Mn^{4+} ion) and the B sites (Mn^{3+} ions), play an important role in stabilizing the distorted cubane geometry of the $[Mn^{4+}Mn^{3+}_3(\mu_3\text{-}O^{2-})_3(\mu_3\text{-}Cl^-)]$ core. Each dbm group forms two coordinate bonds to complete the distorted octahedral geometry at each B site.

Table 1. This table shows the stability of bond lengths (Å) and bond angles (deg) of the $[Mn^{4+}Mn^{3+}_3(\mu_3\text{-}O^{2-})_3(\mu_3\text{-}Cl^-)]$ core by substituting dbm with $CH(CHO)_2$. The relative changes (%) in bond lengths and bond angles are very small.

	Mn_4-dbm	Mn_4–$CH(CHO)_2$	%
Mn^{4+}-(μ_3-O^{2-})-Mn^{3+}	94.940	94.913	0.03
Mn^{4+}-Mn^{3+}	2.844	2.841	0.11
Mn^{4+}-(μ_3-O^{2-})	1.907	1.909	0.11
Mn^{3+}-(μ_3-O^{2-})	1.951	1.947	0.21

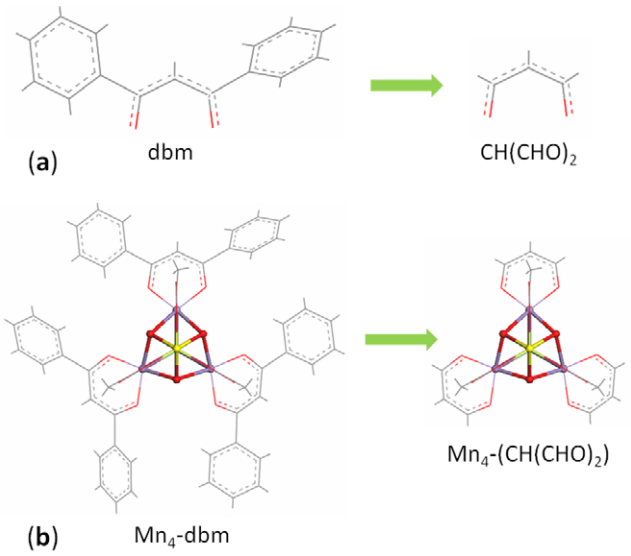

Figure 2. Schematic representation of the pruning procedure adopted for the Mn_4-dbm molecule.

3.1. Modeling Mn_4 molecules

In this study, new distorted cubane $Mn^{4+}Mn^{3+}_3$ molecules were designed by rational variations in the μ_3-O, μ_3-Cl, O_2CMe, and dbm groups of the synthesized distorted cubane Mn_4-dbm molecule.

The Mn_4-dbm molecule contains three dbm groups [12]. Each dbm group, $(CH(COC_6H_5)_2)$, contains two C_6H_5 rings, as depicted in figure 2(a). When replacing each C_6H_5 ring with an isovalent H atom, i.e. substituting $CH(COC_6H_5)_2$ with $CH(CHO)_2$ (a procedure also known as 'hydrogen saturation'), the Mn_4-dbm molecule resizes to $Mn^{4+}Mn^{3+}_3(\mu_3\text{-}O^{2-})_3(\mu_3\text{-}Cl^-)(O_2CMe)^-_3(CH(CHO)_2)^-_3$ (hereafter Mn_4-$CH(CHO)_2$) molecule (see panel (b) of figure 2). Our calculated results show that, with this variation in the dbm groups, the geometric structure of the $[Mn^{4+}Mn^{3+}_3(\mu_3\text{-}O^{2-})_3(\mu_3\text{-}Cl^-)]$ core is nearly unchanged, especially the geometric structure of the Mn^{4+}–(μ_3-O^{2-})–Mn^{3+} exchange pathways, as shown in table 1. Also, the calculated magnetic moments at the Mn^{4+} (m_A) and Mn^{3+} (m_B) ions, as well as the exchange coupling between them (J_{AB}), are nearly constant with this variation in the dbm group, as shown in table 2. These results demonstrate that variation in the outer part of dbm groups is not so much an influence on the magnetic properties of $Mn^{4+}Mn^{3+}_3$ molecules. This finding is very helpful, since the computational cost can be significantly reduced. Next, new distorted cubane $Mn^{4+}Mn^{3+}_3$ will be designed based on the Mn_4–$CH(CHO)_2$ molecule instead of the Mn_4-dbm molecule.

Table 2. This table shows the stability of magnetic moments (in μ_B unit) at Mn^{4+} (m_A) and Mn^{3+} (m_B) ions, as well as J_{AB} by substituting dbm with $CH(CHO)_2$. The relative changes (%) in magnetic moments and J_{AB} are very small.

	Mn_4-dbm	Mn_4–$CH(CHO)_2$	%
m_A	−2.722	−2.717	0.18
m_B	3.874	3.891	0.44
J_{AB}/k_B (K)	−71.33	−70.67	0.48

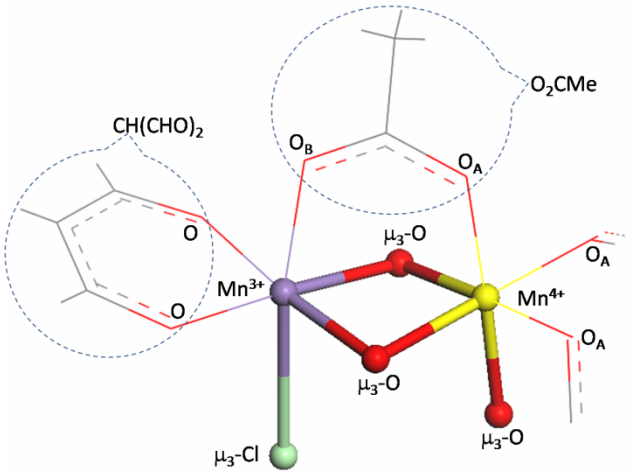

Figure 3. Schematic representation of the ligand configuration at the Mn^{3+} and Mn^{4+} sites of the $Mn^{4+}Mn^{3+}_3(\mu_3\text{-}O^{2-})_3(\mu_3\text{-}Cl^-)(O_2CMe)^-_3(CH(CHO)_2)^-_3$ molecule (the atoms in the $[Mn^{4+}Mn^{3+}_3(\mu_3\text{-}O^{2-})_3(\mu_3\text{-}Cl^-)]$ core are highlighted in the ball).

In the Mn_4–$CH(CHO)_2$ molecule, the μ_3-O atoms form Mn^{4+}–(μ_3-O^{2-})–Mn^{3+} exchange pathways between the Mn^{4+} and Mn^{3+} ions, as shown in figure 3. Therefore, substituting μ_3-O with other ligands will be an effective way to tailor the geometric structure of exchange pathways between the Mn^{4+} and Mn^{3+} ions, as well as the exchange coupling between them. To preserve the distorted cubane geometry of the core of $Mn^{4+}Mn^{3+}_3$ molecules and the formal charges of Mn ions, ligands substituted for the core μ_3-O ligand should satisfy the following conditions: (i) to have the valence of 2; (ii) the ionic radius of these ligands should be not so different from that of O^{2-} ion. From these remarks, N based ligands, NR′ (R′ = a radical), should be the best candidates. Moreover, by varying the R′ group, the local electronic structure as well as electronegativity at the N site can be controlled. As a consequence, the Mn–N bond lengths and the Mn^{4+}–N–Mn^{3+} angles (α), as well as delocalization of d_{z^2} electrons from the Mn^{3+} sites to the Mn^{4+} site and J_{AB}, are expected to be tailored. Also, by varying the core μ_3-Cl ligand and the O_2CMe ligands, the local electronic structures at the Mn sites are also changed. Therefore, combining variations in μ_3-O, μ_3-Cl and O_2CMe ligands is expected to be an effective way to seek new superior $Mn^{4+}Mn^{3+}_3$ SMMs with strong J_{AB}, as well as to reveal magneto-structural correlations of $Mn^{4+}Mn^{3+}_3$ SMMs. By combining variations in μ_3-O, μ_3-Cl and O_2CMe ligands, forty two new $Mn^{4+}Mn^{3+}_3$ molecules have been designed. These molecules have a general chemical formula $[Mn^{4+}Mn^{3+}_3(\mu_3\text{-}L^{2-})_3(\mu_3\text{-}X^-)Z^{3-}(CH(CHO)_2)^-_3]$ (hereafter Mn_4L_3XZ) with L = O, NH, NCH_3, NCH_2–CH_3, NCH = CH_2, NC ≡ CH, or NC_6H_5; X = F, Cl, or Br; and

Table 3. The chemical formulae of Mn_4L_3XZ molecules and their ligands.

	L	X	Z	Chemical formula of Mn_4L_3XZ molecules
1	O	F		$Mn_4O_3F(O_2CMe)_3(CH(CHO)_2)_3$
2		Cl	Z1	$Mn_4O_3Cl(O_2CMe)_3(CH(CHO)_2)_3$
3		Br		$Mn_4O_3Br(O_2CMe)_3(CH(CHO)_2)_3$
4		F		$Mn_4O_3F(MeC(CH_2NOCMe)_3)(CH(CHO)_2)_3$
5		Cl	Z2	$Mn_4O_3Cl(MeC(CH_2NOCMe)_3)(CH(CHO)_2)_3$
6		Br		$Mn_4O_3Br(MeC(CH_2NOCMe)_3)(CH(CHO)_2)_3$
7	NH	F		$Mn_4(NH)_3F(O_2CMe)_3(CH(CHO)_2)_3$
8		Cl	Z1	$Mn_4(NH)_3Cl(O_2CMe)_3(CH(CHO)_2)_3$
9		Br		$Mn_4(NH)_3Br(O_2CMe)_3(CH(CHO)_2)_3$
10		F		$Mn_4(NH)_3F(MeC(CH_2NOCMe)_3)(CH(CHO)_2)_3$
11		Cl	Z2	$Mn_4(NH)_3Cl(MeC(CH_2NOCMe)_3)(CH(CHO)_2)_3$
12		Br		$Mn_4(NH)_3Br(MeC(CH_2NOCMe)_3)(CH(CHO)_2)_3$
13	NCH_3	F		$Mn_4(NCH_3)_3F(O_2CMe)_3(CH(CHO)_2)_3$
14		Cl	Z1	$Mn_4(NCH_3)_3Cl(O_2CMe)_3(CH(CHO)_2)_3$
15		Br		$Mn_4(NCH_3)_3Br(O_2CMe)_3(CH(CHO)_2)_3$
16		F		$Mn_4(NCH_3)_3F(MeC(CH_2NOCMe)_3)(CH(CHO)_2)_3$
17		Cl	Z2	$Mn_4(NCH_3)_3Cl(MeC(CH_2NOCMe)_3)(CH(CHO)_2)_3$
18		Br		$Mn_4(NCH_3)_3Br(MeC(CH_2NOCMe)_3)(CH(CHO)_2)_3$
19	NCH_2-CH_3	F		$Mn_4(NC_2H_5)_3F(O_2CMe)_3(CH(CHO)_2)_3$
20		Cl	Z1	$Mn_4(NC_2H_5)_3Cl(O_2CMe)_3(CH(CHO)_2)_3$
21		Br		$Mn_4(NC_2H_5)_3Br(O_2CMe)_3(CH(CHO)_2)_3$
22		F		$Mn_4(NC_2H_5)_3F(MeC(CH_2NOCMe)_3)(CH(CHO)_2)_3$
23		Cl	Z2	$Mn_4(NC_2H_5)_3Cl(MeC(CH_2NOCMe)_3)(CH(CHO)_2)_3$
24		Br		$Mn_4(NC_2H_5)_3Br(MeC(CH_2NOCMe)_3)(CH(CHO)_2)$
25	$NCH=CH_2$	F		$Mn_4(NC_2H_3)_3F(O_2CMe)_3(CH(CHO)_2)_3$
26		Cl	Z1	$Mn_4(NC_2H_3)_3Cl(O_2CMe)_3(CH(CHO)_2)_3$
27		Br		$Mn_4(NC_2H_3)_3Br(O_2CMe)_3(CH(CHO)_2)_3$
28		F		$Mn_4(NC_2H_3)_3F(MeC(CH_2NOCMe)_3)(CH(CHO)_2)_3$
29		Cl	Z2	$Mn_4(NC_2H_3)_3Cl(MeC(CH_2NOCMe)_3)(CH(CHO)_2)_3$
30		Br		$Mn_4(NC_2H_3)_3Br(MeC(CH_2NOCMe)_3)(CH(CHO)_2)_3$
31	$NC\equiv CH$	F		$Mn_4(NCH)_3F(O_2CMe)_3(CH(CHO)_2)_3$
32		Cl	Z1	$Mn_4(NCH)_3Cl(O_2CMe)_3(CH(CHO)_2)_3$
33		Br		$Mn_4(NCH)_3Br(O_2CMe)_3(CH(CHO)_2)_3$
34		F		$Mn_4(NCH)_3F(MeC(CH_2NOCMe)_3)(CH(CHO)_2)_3$
35		Cl	Z2	$Mn_4(NCH)_3Cl(MeC(CH_2NOCMe)_3)(CH(CHO)_2)_3$
36		Br		$Mn_4(NCH)_3Br(MeC(CH_2NOCMe)_3)(CH(CHO)_2)_3$
37	NC_6H_5	F		$Mn_4(NC_6H_5)_3F(O_2CMe)_3(CH(CHO)_2)_3$
38		Cl	Z1	$Mn_4(NC_6H_5)_3Cl(O_2CMe)_3(CH(CHO)_2)_3$
39		Br		$Mn_4(NC_6H_5)_3Br(O_2CMe)_3(CH(CHO)_2)_3$
40		F		$Mn_4(NC_6H_5)_3F(MeC(CH_2NOCMe)_3)(CH(CHO)_2)_3$
41		Cl	Z2	$Mn_4(NC_6H_5)_3Cl(MeC(CH_2NOCMe)_3)(CH(CHO)_2)_3$
42		Br		$Mn_4(NC_6H_5)_3Br(MeC(CH_2NOCMe)_3)(CH(CHO)_2)_3$

$Z1 = (O_2CMe)_3$, $Z2 = MeC(CH_2NOCMe)_3$.

$Z = (O_2CMe)_3$ or $MeC(CH_2–NOCMe)_3$. These 42 Mn_4L_3XZ molecules are labeled **1** to **42**, and their chemical formulae are given in table 3.

3.2. The geometric and electronic structures

To determine exactly the magnetic ground state of Mn_4L_3XZ molecules, the same computational method as in our previous paper was used [5]. In this method, all possible spin configurations of Mn_4L_3XZ molecules are probed, which are imposed as an initial condition of the structural optimization procedure. The number of spin configurations should be considered depending on the charge state of manganese ions. In terms of the octahedral field, Mn^{4+} ions could, in principle, have only the high-spin state with the configuration $d^3(t_{2g}^3, e_g^0)$, in which three d electrons occupy three different t_{2g} orbitals. The possible spin states of the Mn^{3+} ion are the high-spin (HS) state with configuration $d^4(t_{2g}^3, e_g^1)$ and the low-spin (LS) state with configuration $d^4(t_{2g}^4, e_g^0)$. Additionally, the magnetic coupling between the Mn^{4+} ion at the A site and Mn^{3+} ions at the B site can be ferromagnetic (FM) or antiferromagnetic (AFM). Therefore, there are four spin configurations that should be considered for each Mn_4L_3XZ molecule, including (i) AFM-HS, (ii) AFM-LS, (iii) FM-HS and (iv) FM-LS. Our calculated results show that the most magnetic stable state of all 42 Mn_4L_3XZ molecules is the AFM-HS. This means that

Table 4. Selected important magnetic and geometric parameters of 42 Mn_4L_3XZ molecules, the effective exchange coupling parameter between the Mn^{4+} and Mn^{3+} ions (J_{AB}/k_B in K), the magnetic moment at Mn sites (m_A and m_B in μ_B), the strength of delocalization of 3d electrons $\Delta m_A = 3 - |m_A|$, the exchange coupling angle A-L-B (α in degree), the distance between the Mn^{4+} and Mn^{3+} ions (d_{AB} in Å), the $Mn^{3+}O_B$ and $Mn^{3+}O$ bond lengths (d_Z and d_{XY} in Å), and the distortion factor of B sites (f_{dist} in %).

	L	X	Z	m_A	m_B	Δm_A	J_{AB}/k_B	α	d_{AB}	d_Z	d_{XY}	f_{dist}
1	O	F		−2.692	3.907	0.308	−75.15	95.06	2.840	1.994	2.195	10.1
2		Cl	Z1	−2.717	3.891	0.283	−70.67	94.91	2.841	1.992	2.193	10.1
3		Br		−2.719	3.876	0.281	−69.72	94.83	2.841	1.992	2.193	10.1
4		F		−2.674	3.890	0.326	−75.16	95.21	2.854	2.007	2.142	6.7
5		Cl	Z2	−2.681	3.871	0.319	−73.21	95.47	2.864	2.005	2.134	6.4
6		Br		−2.675	3.855	0.325	−73.28	95.36	2.864	2.005	2.127	6.1
7	NH	F		−2.719	3.919	0.281	−86.29	94.35	2.876	2.016	2.231	10.7
8		Cl	Z1	−2.768	3.915	0.232	−62.64	94.58	2.888	2.011	2.222	10.5
9		Br		−2.763	3.901	0.237	−61.17	94.43	2.885	2.011	2.217	10.2
10		F		−2.616	3.888	0.384	−122.09	94.04	2.869	2.027	2.173	7.2
11		Cl	Z2	−2.655	3.886	0.345	−93.64	94.50	2.889	2.026	2.155	6.4
12		B		−2.655	3.875	0.345	−88.64	94.58	2.892	2.025	2.149	6.1
13	NCH_3	F		−2.566	3.917	0.434	−161.40	91.24	2.820	2.028	2.255	11.2
14		Cl	Z1	−2.609	3.911	0.391	−134.85	91.33	2.828	2.029	2.235	10.2
15		Br		−2.627	3.900	0.373	−125.10	91.39	2.831	2.026	2.239	10.5
16		F		−2.419	3.884	0.581	−209.07	91.06	2.819	2.040	2.187	7.2
17		Cl	Z2	−2.490	3.886	0.510	−163.09	91.72	2.843	2.040	2.170	6.4
18		Br		−2.492	3.873	0.508	−155.39	91.71	2.845	2.039	2.163	6.1
19	$NCH_2 - CH_3$	F		−2.543	3.909	0.457	−174.47	89.77	2.798	2.032	2.252	10.9
20		Cl	Z1	−2.629	3.910	0.371	−134.93	90.02	2.816	2.031	2.246	10.6
21		Br		−2.651	3.899	0.349	−124.27	90.32	2.823	2.028	2.244	10.6
22		F		−2.396	3.878	0.604	−214.79	89.69	2.802	2.045	2.177	6.5
23		Cl	Z2	−2.503	3.886	0.497	−162.12	90.43	2.830	2.044	2.170	6.2
24		Br		−2.527	3.877	0.473	−149.50	90.57	2.836	2.043	2.168	6.1
25	$NCH = CH_2$	F		−2.615	3.990	0.385	−108.46	91.30	2.860	2.027	2.232	10.1
26		Cl	Z1	−2.676	3.988	0.324	−83.18	91.59	2.874	2.026	2.221	9.7
27		Br		−2.691	3.975	0.309	−75.81	91.65	2.878	2.025	2.217	9.5
28		F		−2.531	3.969	0.469	−135.92	91.30	2.868	2.036	2.176	6.9
29		Cl	Z2	−2.590	3.969	0.410	−104.50	91.87	2.890	2.037	2.148	5.4
30		Br		−2.603	3.957	0.397	−96.38	92.00	2.895	2.038	2.152	5.6
31	$NC \equiv CH$	F		−2.809	4.018	0.191	−63.23	93.05	2.944	2.009	2.207	9.9
32		Cl	Z1	−2.887	4.011	0.113	−41.73	93.34	2.959	2.008	2.198	9.5
33		Br		−2.903	3.999	0.097	−36.77	93.37	2.963	2.007	2.196	9.4
34		F		−2.625	3.983	0.375	−102.53	92.27	2.926	2.019	2.136	5.8
35		Cl	Z2	−2.720	3.988	0.280	−70.38	93.27	2.961	2.017	2.130	5.6
36		Br		−2.730	3.976	0.270	−64.43	93.41	2.967	2.018	2.125	5.3
37	NC_6H_5	F		−2.469	3.966	0.531	−163.25	88.84	2.831	2.035	2.191	7.7
38		Cl	Z1	−2.558	3.974	0.442	−127.51	89.41	2.853	2.030	2.196	8.2
39		Br		−2.573	3.965	0.427	−116.75	89.63	2.861	2.035	2.191	7.7
40		F		−2.416	3.943	0.584	−178.58	88.90	2.845	2.042	2.140	4.8
41		Cl	Z2	−2.505	3.957	0.495	−134.77	90.04	2.888	2.042	2.129	4.3
42		Br		−2.524	3.951	0.476	−122.58	90.31	2.898	2.042	2.125	4.1

$Z1 = (O_2CMe)_3$, $Z2 = MeC(CH_2NOCMe)_3$.

the three Mn^{3+} ions at the B sites exist in the HS state with configuration $d^4(t_{2g}^3, e_g^1)$, and the exchange coupling between the three Mn^{3+} ions and the Mn^{4+} ion is AFM, resulting in the ferrimagnetic structure in Mn_4L_3XZ molecules with the large S_T of 9/2.

Note that the HS state with configuration $d^4(t_{2g}^3, e_g^1)$ relates to the appearance of Jahn–Teller distortions at Mn^{3+} ions. Our calculated results confirm that each of three Mn^{3+} sites is an elongated octahedron along the $Mn^{3+}O_B$ axis. Here, the distortion factor of the B sites is measured by

$$f_{dist} = \frac{d_Z - d_{XY}}{d_{XY}} \cdot 100\%, \quad (1)$$

where d_Z is the interatomic distance between the Mn^{3+} and O_B sites, as labeled in figure 3. The d_{XY} is the average interatomic distance between the Mn^{3+} site and the two O sites of the $CH(CHO)_2$ group, as shown in figure 3. The value of f_{dist} is given in table 4, in which molecule **13** with [L, X, Z] = [NCH_3, F, $(O_2CMe)_3$] has the highest value of

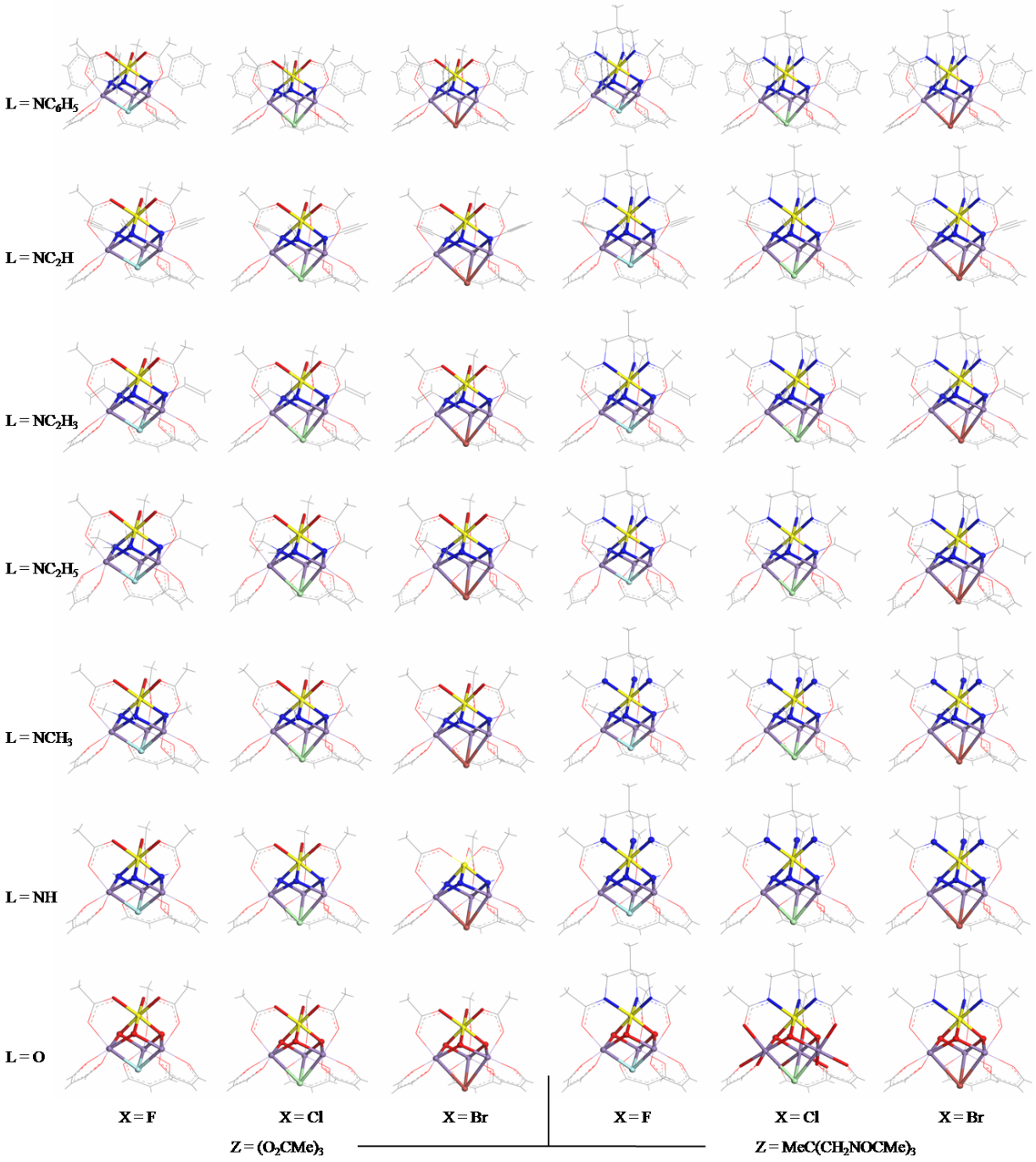

Figure 4. The schematic geometric structure of 42 Mn_4L_3XZ molecules. This figure also illustrates the development of geometric structure of Mn_4L_3XZ molecules by variations in L, X and Z ligands. Color codes: Mn^{3+} (violet), Mn^{4+} (yellow), O (red), N (blue), C (grey), F (light turquoise), Cl (light green) and Br (brown).

$f_{\text{dist}} = 11.2\%$, the molecule **42** with [L, X, Z] = [NC_6H_5, Br, and $MeC(CH_2{-}NOCMe)_3$] has the smallest value of $f_{\text{dist}} = 4.1\%$. The HS spin state as well as the elongated Jahn–Teller distortions at Mn^{3+} ions is known as one of the origins of the axial anisotropy in Mn SMMs [20−22]. These results demonstrate that all 42 Mn_4L_3XZ molecules must have axial anisotropy. Therefore, they are high-spin anisotropic molecules. Next, we will present in detail about the geometric structure and magnetic properties of these 42 Mn_4L_3XZ molecules. The geometric structures corresponding to the most stable states of these 42 Mn_4L_3XZ molecules are depicted in figure 4. Figure 4 also illustrates the development of geometric structure of Mn_4L_3XZ molecules by variations in L, X and Z ligands. Our calculations confirm that the C_{3v} symmetry of Mn_4L_3XZ molecules, with the C_{3v} axis passing through the A and X sites, is preserved even if the L, X and Z ligands are changed. Also, the distorted cubane geometry of the Mn_4L_3X core is preserved. However, their bond angles and interatomic distances are various, in which the exchange coupling angle (α) and the Mn^{3+}–Mn^{4+} interatomic distance (d_{AB}) are changed in the ranges of 88.84°–95.47° and 2.798–2.967 Å, respectively, as shown in table 4. As expected, the J_{AB} is also various, as shown in table 4. The calculated results confirm the expectation that

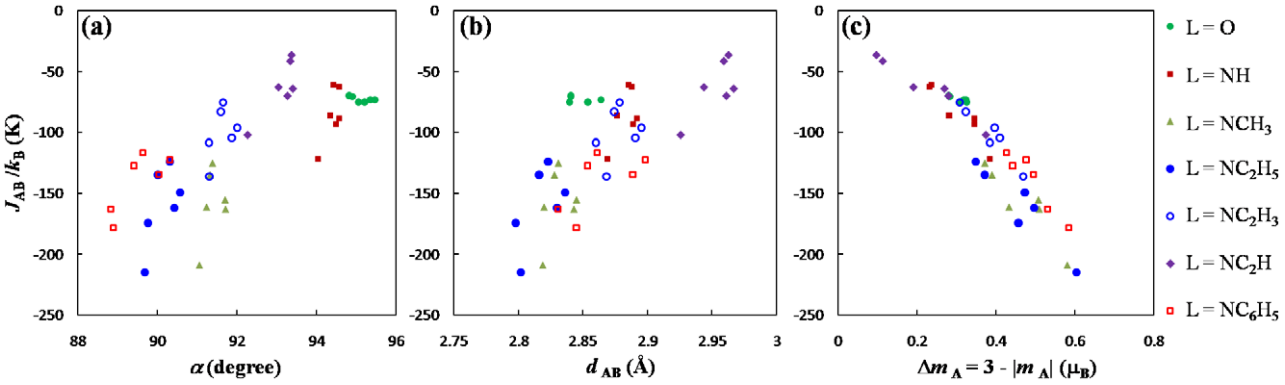

Figure 5. From left to right: (a) the α dependence of J_{AB}, (b) the d_{AB} dependence of J_{AB}, and (c) the Δm_A dependence of J_{AB}.

J_{AB} tends to become stronger when the α reaches around 90°, as demonstrated in figure 5(a), due to the enhancement of hybridization between 3d orbitals at Mn sites and ligand orbitals at L sites. The molecule **22** with L = NC_2H_5 has the highest J_{AB}/k_B of −214.79 K, corresponding to $\alpha = 89.69°$. This value is about three times larger than that of molecules **1**–**6** with L = O. Also, the J_{AB} tends to become stronger with a decrease in d_{AB}, which can be attributed to an increase in direct overlap between 3d orbitals at the A and B sites, as shown in figure 5(b).

The α and d_{AB} dependence of J_{AB} demonstrates that, in the space of $88° \leqslant \alpha \leqslant 92°$ and $d_{AB} \leqslant 2.850$ Å (hereafter the strong J_{AB} space), the J_{AB} of Mn_4L_3XZ molecules is at least about twice as strong as that of synthesized Mn_4 SMMs (or Mn_4 molecules with L = O). Here it is noted that, in the strong J_{AB} space, there are many Mn_4L_3XZ molecules with L being N-based ligands, such as L = NCH_3, NC_2H_5 and NC_6H_5, while Mn_4L_3XZ molecules with L = O is far from this space. These results demonstrate the advantages of using N-based ligands instead of oxygen to form exchange pathways between Mn ions. N-based ligands give us possibilities of designing new superior $Mn^{4+}Mn^{3+}_3$ molecules with a strong J_{AB}.

3.3. Relation between Mn–Mn exchange coupling and delocalization of 3d electrons

As discussed above, J_{AB} can be described pretty well by the geometric parameters α and d_{AB}. However, as discussed in our previous paper [5], the basic mechanism of exchange coupling between the Mn^{4+} and Mn^{3+} ions in distorted cubane $Mn^{4+}Mn^{3+}_3$ molecules results from delocalization of the d_{z^2} electrons from the Mn^{3+} ions to the Mn^{4+} ion, which can be evaluated by a difference between the formal magnetic moment and calculated magnetic moment of the Mn^{4+} ion, $\Delta m_A = 3 - |m_A|$ (where m_A is the calculated magnetic moment of the Mn^{4+} ion). The values of Δm_A of 42 Mn_4L_3XZ molecules are given in table 4. It is expected that the larger Δm_A, the stronger J_{AB}. The Δm_A dependence of J_{AB} of Mn_4L_3XZ molecules, which is plotted in figure 5(c), confirms this expectation. As illustrated in figure 5(c), our calculated results demonstrate a very linear relation between Δm_A and J_{AB},

$$J_{AB}/k_B = -350.68\Delta m_A + 20.23, \qquad (2)$$

with the coefficient of determination $R^2 = 0.87$. This finding suggests an effective way to predict J_{AB} of distorted cubane $Mn^{4+}Mn^{3+}_3$ molecules. A comparison among figures 5(a)−(c) shows that Δm_A is a much better parameter to describe J_{AB} than α and d_{AB}.

4. Conclusion

By rational variations in the μ_3-O, μ_3-Cl, O_2CMe and dbm groups of synthesized distorted cubane $Mn^{4+}Mn^{3+}_3(\mu_3\text{-}O^{2-})_3(\mu_3\text{-}Cl^-)(O_2CMe)^-_3(dbm)^-_3$ molecules, 42 new anisotropic high-spin distorted cubane $Mn^{4+}Mn^{3+}_3$ (Mn_4L_3XZ) molecules have been designed with ferrimagnetic structures between the Mn^{4+} and Mn^{3+} ions resulting in S_T of 9/2. These 42 Mn_4L_3XZ molecules having the Mn^{4+}–L–Mn^{3+} exchange coupling angle (α) and the Mn^{3+}–Mn^{4+} interatomic distance (d_{AB}) are various in the ranges of 88.84°–95.47° and 2.798−2.967 Å, respectively. The calculated results demonstrate that, J_{AB} tends to become stronger when α reaches around 90°. The molecule **22** has the highest J_{AB}/k_B of −214.79 K corresponding to $\alpha = 89.69°$. This value is about three times larger than that of synthesized Mn_4 SMMs. The J_{AB} also tends to become stronger when d_{AB} decreases. These magnetostructural correlations demonstrate that the condition for a $Mn^{4+}Mn^{3+}_3$ molecule to have strong J_{AB} is that this $Mn^{4+}Mn^{3+}_3$ molecule has to have α around 90° and short enough d_{AB}. Our calculated results show that, in the space of $\{88° \leqslant \alpha \leqslant 92°$ and $d_{AB} \leqslant 2.850$ Å$\}$, J_{AB} of Mn_4L_3XZ molecules under study is at least about twice as strong as that of synthesized $Mn^{4+}Mn^{3+}_3$ SMMs. In this space, there are many Mn_4L_3XZ molecules with L being N-based ligands, such as NCH_3, NC_2H_5 and NC_6H_5, while there is no Mn_4L_3XZ molecule with L = O in this space. These results demonstrate the advantages of using N-based ligands to form exchange pathways between manganese ions. N-based ligands give us possibilities of designing new superior $Mn^{4+}Mn^{3+}_3$ molecules with strong J_{AB}. A new magnetic parameter that can depict delocalization of 3d electrons between Mn sites, $\Delta m_A = 3 - |m_A|$, has been introduced. The Δm_A dependence of J_{AB} demonstrates a very linear relation. We hope that these results will give some hints for synthesizing not only new superior $Mn^{4+}Mn^{3+}_3$ SMMs but also other SMM systems.

Acknowledgments

We thank the Vietnam's National Foundation for Science and Technology Development (NAFOSTED) for funding this work within project 103.01.77.09. The computations presented in this study were performed at the Information Science Center of Japan's Advanced Institute of Science and Technology, and the Center for Computational Science of the Faculty of Physics, Hanoi University of Science, Vietnam.

References

[1] Bogani L and Wernsdorfer W 2008 *Nat. Mater.* **7** 179
[2] Friedman J R, Sarachik M P, Tejada J and Ziolo R 1996 *Phys. Rev. Lett.* **76** 3830
Thomas L, Lionti L, Ballou R, Gatteschi D, Sessoli R and Barbara B 1996 *Nature* **383** 145
[3] Saitoh, Miyasaka H, Yamashita M and Clérac R 2007 *J. Mater. Chem.* **17** 2002
Marvaud V, Herrera J M, Barilero T, Tuyeras F, Garde R, Scuiller A, Decroix C, Cantuel M and Desplanches C 2003 *Monatshefte für Chem.* **134** 149
Milios C J, Vinslava A, Wernsdorfer W, Moggach S, Parsons S, Perlepes S P, Christou G and Brechin E K 2007 *J. Am. Chem. Soc.* **129** 2754
[4] Inglis R, Taylor S M, Jones L F, Papaefstathiou G S, Perlepes S P, Datta S, Hill S, Wernsdorfer W and Brechin E K 2009 *Dalton Trans.* **42** 9157
Ako A M, Mereacre V, Hewitt I J, Clérac R, Lecren L, Anson C E and Powell A K 2006 *J. Mater. Chem.* **16** 2579
[5] Tuan N A, Katayama S and Chi D H 2009 *Phys. Chem. Chem. Phys.* **11** 717
[6] Tuan N A, Katayama S and Chi D H 2008 *Comput. Mater. Sci.* **44** 111
Han M J, Ozaki T and Yu J 2004 *Phys. Rev.* B **70** 184421
Park K, Pederson M R, Richardson S L, Alcalde N A and Christou G 2003 *Phys. Rev.* B **68** 020405
Park K, Pederson M R and Bernstein N 2004 *J. Phys. Chem. Solids* **65** 805
[7] Bashkin J S, Chang H, Streib W E, Huffman J C, Hendricson D N and Christou G 1987 *J. Am. Chem. Soc.* **109** 6502
[8] Wang S, Filting K, Streib W E, Schmitt E A, McCusker J K, Hendrickson D N and Christou G 1991 *Angew. Chem., Int. Ed. Engl.* **30** 305
[9] Hendrickson N *et al* 1992 *J. Am. Chem. Soc.* **114** 2455
[10] Li Q, Vincent J B, Libby E, Chang H, Huffman J C, Boyd P D W, Christou C and Hendrickson D N 1988 *Angew. Chem., Int. Ed. Engl.* **27** 1731
[11] Wemple M W, Tsai H, Folting K, Hendrickson D N and Christou G 1993 *Inorg. Chem.* **32** 2025
[12] Wang S, Tsai H, Libby E, Folting K, Streib W E, Hendrickson D N and Christou G 1996 *Inorg. Chem.* **35** 7578
[13] Andres H, Basler R, Güdel H, Aromí G, Christou G, Büttner H and Rufflé B 2000 *J. Am. Chem. Soc.* **122** 12469
[14] Aubin S M J, Dilley N R, Pardi L, Krzystek J, Wemple M W, Brunel L, Maple M B, Christou G and Hendrickson D N 1998 *J. Am. Chem. Soc.* **120** 4991
[15] Wernsdorfer W, Aliaga-Alcalde N, Hendrickson D N and Christou G 2002 *Nature* **416** 406
[16] Delley B 1990 *J. Chem. Phys.* **92** 508
[17] Hammer B, Hansen L B and Norskov J K 1999 *Phys. Rev.* B **59** 7413
[18] Delley B 1998 *Int. J. Quantum Chem.* **69** 423
[19] Mulliken R S 1955 *J. Chem. Phys.* **23** 1833
Mulliken R S 1955 *J. Chem. Phys.* **23** 1841
[20] Sessoli R, Tsai H L, Schake A R, Wang S, Vincent J B, Folting K, Gatteschi D, Christou G and Hendrickson D N 1993 *J. Am. Chem. Soc.* **115** 1804
[21] Yang C I, Wernsdorfer W, Lee G H and Tsai H L 2007 *J. Am. Chem. Soc.* **129** 456
[22] Miyasaka H, Madanbashi T, Sugimoto K, Nakazawa Y, Wernsdorfer W, Sugiura K, Yamashita M, Coulon C and Clérac R 2006 *Chem. Eur. J.* **12** 7028